Electrochimica Acta 78 (2012) 109–114

Contents lists available at SciVerse ScienceDirect

Electrochimica Acta

journal homepage: www.elsevier.com/locate/electacta

Activated direct electron transfer of nanoAu bioconjugates of cytochrome c for electrocatalytic detection of trace levels of superoxide dismutase enzyme

K. Koteshwara Reddy, K. Vengatajalabathy Gobi*

Department of Chemistry, National Institute of Technology, Warangal, Andhra Pradesh 506004, India

ARTICLE INFO

Article history:
Received 7 March 2012
Received in revised form 9 May 2012
Accepted 10 May 2012
Available online 17 June 2012

Keywords:
Superoxide dismutase
Biosensor
NanoAu particles
Cytochrome c
Self-assembly
Transmission electron microscope
Amperometry
NanoAu surface morphology

ABSTRACT

A novel amperometric biosensor for the detection of trace levels of superoxide dismutase enzyme is developed with the use of nanoAu bioconjugates of cytochrome c (Cyt c). NanoAu particles of finite size were synthesized by borohydride reduction in the presence of alkanethiols having —COOH and —OH end groups. The nanoAu particles were characterized by transmission electron microscopic analysis, and the mean size of the nanoparticles is determined to be 2.96 nm diameter. The heme protein, Cyt c, is bound to the nanoAu particles, and the resulting nanoAu bioconjugates are investigated by cyclic voltammetric and rotating-disk voltammetric experiments. Cyt c has become electrodically reactive by binding with the nanoAu particles, and Cyt c-bound nanoAu particles exhibited a reversible, mass-transport limited electron-transfer reaction. Reversible redox peaks are observed with the formal redox potential of +0.05 V (vs. Ag|AgCl) at bare GC and also at Au|alkanethiolate monolayer electrodes. Cyt c is highly reactive to superoxide radical, and electrocatalytic oxidation of superoxide occurs at the applied potential of +0.15 V in the presence of the nanoAu bioconjugates. Steady state current–time curves show a sharp increase in the anodic current to the generation of superoxide radical and attain a plateau in ca. 6 min. The structure and morphology of the alkanethiolate layer at the nanoAu-Cyt c interface tremendously influences the electrocatalytic current for superoxide. The electrocatalytic current observed for superoxide radical varied sharply by the presence of superoxide dismutase. From the dependence of the electrocatalytic current for superoxide on the concentration of superoxide dismutase, a low-detection-limit of as low as 0.25 U mL^{-1} (~50 ng mL^{-1}) has been established.

© 2012 Elsevier Ltd. All rights reserved.

1. Introduction

Superoxide radical is highly reactive and is continuously generated during cell respiration and metabolism. It plays an important role in the destruction of microorganisms invading into our body. It is however frequently observed that high amounts of superoxide formation can exceed the antioxidant abilities of cells and may be involved in oxidative damage to tissues, nerve cells, etc. Such excessive generation of superoxide leads to the development of various pathologies such as cardiovascular dysfunction, arteriosclerosis, ischemia, and critical neurodegenerative diseases. Superoxide dismutase enzyme (SOD) plays a major protective role in living cells and has been widely used as a pharmacological tool in the study of pathophysiological mechanisms. Ubiquitous presence of SOD throughout the evolutionary chain emphasizes its importance, and the detection of SOD enzyme is essential if we are to better control the degenerative processes and to diagnose more accurately the diseases in which it is involved [1–4].

SOD is a potential and selective scavenger of superoxide, and the best way for the detection of SOD thus could be the analysis of superoxide radical. Electrochemical methods are of great importance in the development of sensors because of its potential advantages such as portable instrumentation, in vivo analysis with microprobes, on-line measurement, miniaturization and low equipment cost [5]. Biorecognition elements impart high selectivity and sensitivity to sensors, enabling direct detection of the analyte of interest from complex sample matrices without any purification or pre-concentration steps. Cytochrome c (Cyt c) would undergo facile reductive reaction with superoxide radical, and thus electrochemical sensors for detection of superoxide were constructed with Cyt c as biorecognition element using suitable electron-transfer promoters [6–9]. Mediatorless third-generation biosensors have been fabricated for the detection of superoxide and SOD with the use of monolayer-based functional electrodes. Self-assembled monolayers of alkanethiols with covalently bound Cyt c were investigated for the detection of superoxide radical and SOD. To improve the sensor performances, nanoAu particles of rod-like, spherical, and pyramidal structures [10], nano NiO powder [11], etc. were investigated as the base electrode surface. However, the biorecognition element is limited merely up to a

* Corresponding author. Tel.: +91 870 2462674.
E-mail address: drkvgobi@gmail.com (K. Vengatajalabathy Gobi).

0013-4686/$ – see front matter © 2012 Elsevier Ltd. All rights reserved.
http://dx.doi.org/10.1016/j.electacta.2012.05.159

monolayer level. Thus, three-dimensional macroporous materials [12], sol–gel matrix [13,14], and meticulously fabricated layer-by-layer multilayer assembly [15] have been investigated to increase the active surface area and thus the sensitivity.

Gold nanoparticles have emerged as a new kind of inspiring materials and have been widely used in the modification of various electrodes and in the fabrication of different kinds of biosensor platforms. They could act as electron-transfer relays and thus could promote the heterogeneous electron transfer between the biorecognition element and the electrode [16–20]. Thus, such nanoAu bound biorecognition elements would be immensely useful in fabricating high-performance three-dimensional matrix based electrochemical sensors and would provide added advantages of mediatorless sensors and three-dimensional bulk matrices.

In this investigation, finite nanogold particles passivated with short chain alkanethiols having carboxyl and hydroxyl end groups are synthesized, and Cyt c is bound to the —COOH groups present around of the nanogold particles. The electrochemical characteristics of the nanoAu-Cyt c conjugates are investigated by cyclic voltammetric and rotating-disk voltammetric experiments. Electrocatalytic activity of the nanoAu-Cyt c conjugates with superoxide radical is investigated for the detection of SOD enzyme. Influence of the surface morphology of the nanogold particles on the electrocatalytic activity and thus on the sensor performance are discussed.

2. Experimental

2.1. Reagents

Horse heart cytochrome c (Cyt c), superoxide dismutase (from bovine erythrocytes; 4600 U mg^{-1}) xanthine oxidase (XOD), hydrogen tetrachloroaurate, and 1-ethyl-3-(3-dimethylaminopropyl)carbodiimide (EDAC) were received from Sigma, stored at −20 °C and used as supplied. Sodium borohydride, xanthine, 3-mercaptopropionic acid (MPA), 3-mercaptopropanol (MPO), 2-aminoethanothiol (AET), disodium hydrogen phosphate, sodium dihydrogen phosphate, and solvents used in this study were of analytical grade and were used as supplied from Tokyo Chemical Industry without further purification. Distilled deionized water filtered at last with 0.2 μm pore filter cartridge (resistance = 18 MΩ) was used for all the aqueous solutions.

2.2. NanoAu-Cyt c conjugate preparation

NanoAu particle was prepared by borohydride reduction of gold (III) chloride in non-aqueous solvent according to the Brust method reported elsewhere [21]. Briefly, 0.16 g hydrogen tetrachloroaurate (III) (0.38 mmol) was dissolved in 7 mL water, and 450 mL of methanol, 0.12 g mercaptopropionic acid (MPA; 1.13 mmol), and acetic acid (3 mL) were added to the Au (III) solution. The solution was cooled under stirring in an ice-bath. Sodium borohydride (0.3 g, 8 mmol) dissolved in 10 mL water was added in small portions to the resultant yellowish Au (III) solution under stirring in a period of 90 s, during which the solution turned to dark black-brown color. The mixture was kept under stirring at 5 °C for 3 h and centrifuged (18,000 rpm) to precipitate the nanoAu particles protected with a monolayer of the alkanethiol (MPA). The precipitate was redistributed in methanol and centrifuged to remove the unreacted compounds. The resulting nanoAu particles were dissolved in 25 mM sodium phosphate buffer (pH 8.0) and filtered through nanoporous cellulose filter membrane (Millipore 25 nm cut-off membrane) to remove aggregated large nanoparticles. The nanoAu particles thus prepared was denoted hereafter as nanoAu/MPA. The surface morphology of the nanoparticles was changed by treating nanoAu/MPA with 3-mercaptopropanol (MPO) in PBS for 1 h, and the resultant mixture was dialyzed to prepare nanoAu particles protected with a mixed binary layer of alkanethiols. The nanoAu particles thus prepared are denoted as nanoAu/MPA + MPO. The nanoAu particles were imagined with transmission electron microscope (TEM) analysis. A dilute solution of the nanoparticle in 25 mM PBS (pH 8.0) was spread on amorphous carbon support, dried and rinsed with PBS. The nanoparticles were imagined with a Hitachi HF-2000 TEM analyzer at the magnification of 1.5 million times.

Cyt c was bound to the nanogold particles through electrostatic interaction by adding 12 mg of cytochrome c to 10 mL nanogold solution, and the resultant mixture was filtered through MWCO membrane (30,000 Da; Whatman) to remove excess unbound cytochrome c. The resultant nanogold-Cyt c conjugate in PBS was treated with EDAC (0.3 mg mL^{-1}) for 1 h to bind Cyt c covalently with the nanogold particles. The concentration of Cyt c bound to the nanoAu particles was estimated by determining the amount of Cyt c adsorbed using UV–vis spectroscopy. The resultant covalently bound nanoAu-Cyt c bioconjugates were denoted hereafter as nanoAu/MPA/Cyt c and nanoAu/MPA + MPO/Cyt c.

2.3. Voltammetric and electrocatalytic experiments

Cyclic voltammetric and rotating-disk voltammetric experiments were carried out with a BAS 100B/W electrochemical analyzer using a conventional two-compartment three-electrode cell. GC and Au electrodes of 5.0 mm and 1.6 mm diameter act as working electrodes, a platinum coil as counter electrode and an Ag|AgCl (NaCl satd.) as reference electrode, and the experimental solutions were deaerated with nitrogen for 15 min. Phosphate buffer solution (PBS; pH 7.0) of 25 mM concentration was used as the electrolyte solution. The working electrodes were polished with aqueous slurries of alumina (10 μm, 1 μm, and then 0.05 μm), washed and cleaned with ultra-sonication for 2 min in water. Au working electrodes were then electrochemically polished by potential scanning (scan rate = 10 V s^{-1}) in 0.05 M sulfuric acid from −0.2 V to 1.5 V for 10 min. The resulting Au electrodes were modified with an alkanethiol monolayer by dipping into an ethanol solution of 10 mM alkanethiol (AET, MPA, etc.) for 1 h and rinsed well with ethanol and water. The resulting electrodes were denoted as Au/AET, Au/MPA, etc.

Superoxide radical for electrocatalytic experiments was generated by xanthine-XOD enzymatic reaction to maintain a steady-state concentration of the superoxide radical. In electrocatalytic experiments, the electrolyte solution was oxygen-saturated by bubbling oxygen for 15 min and stirred with magnetic stirrer gently at 200 rpm to perform at hydrodynamic conditions.

3. Results and discussion

3.1. Synthesis of nanoAu particles and TEM analysis

NanoAu particles have been synthesized in this study according to a modified Brust reaction performed in a single-phase non-aqueous solvent. They are covered with a monolayer or mixed-monolayer of alkanethiols having functional end groups —COOH and —OH, which prevents aggregation of the nanoparticles and also promotes the dispersion of the nanoparticles in solution. A dilute solution of the nanoparticles (0.6 mg mL^{-1}) in PBS (pH 7.0) was spread on an amorphous carbon support, and the substrate was dried and rinsed gently with water. The TEM image of nanoAu/MPA bound on an amorphous carbon support is obtained with a magnification of 1.5 million times and is shown in Fig. 1(A). Sphere-shaped discrete nanoparticles of approximately uniform size are seen all throughout the image. The dark black nature of the circular dots

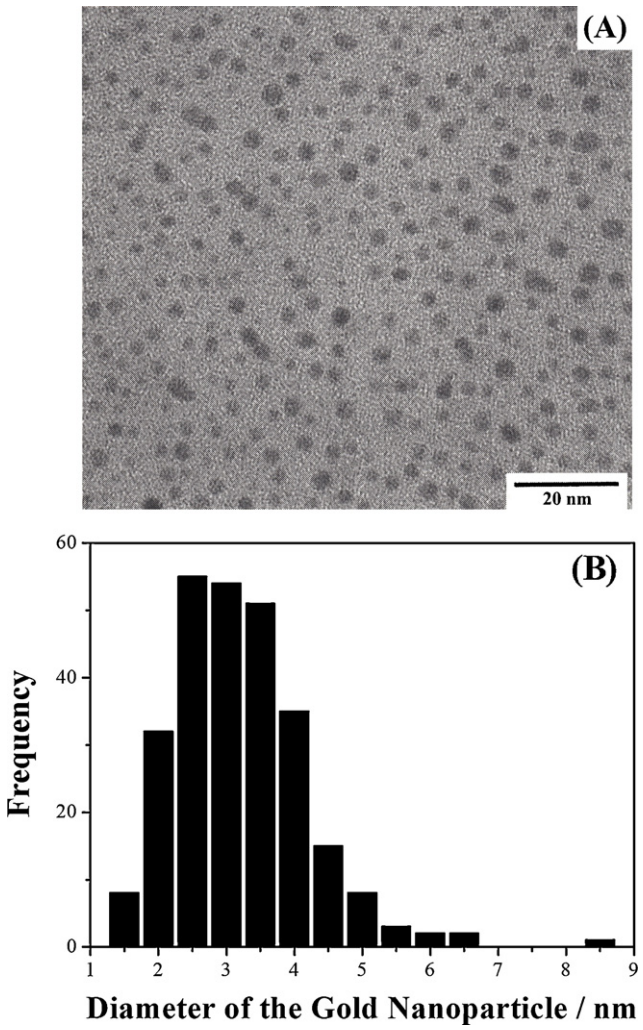

Fig. 1. (A) Transmission electron microscopic (TEM) image of nanoAu/MPA particles supported on an amorphous carbon sheet from a dilute solution of the nanoparticles in PBS (pH 8.0, 25 mM). The image was obtained by recording with a magnification of 1.5 million times, and the scale bar indicates 20 nm. (B) Core-size histogram of nanoAu/MPA particles from TEM measurements. Sizes of ~300 nanoparticles were analyzed.

indicates the poor transmittance and in turn implies that the nanoparticles are of solid spherical shaped compounds. The size of the nanoparticles is determined by core-size histogram analysis from 300 discrete nanoparticles in the image. The distribution of the size of the nanoparticles is shown in Fig. 1(B). The size of the most of the nanoparticles seems to vary in a narrow region of 2.5–3.5 nm, and the mean diameter of the nanoparticles is determined to be 2.96 nm with a standard deviation of ±0.92 nm. It clearly shows that the particles are of finite size with homogeneous nature and uniform surface characteristics.

3.2. Electrochemical investigations of nanoAu-Cyt c conjugates

Cyclic voltammograms (CVs) of the nanoAu-Cyt c conjugates dissolved in solution are investigated at bare GC and at various Au/alkanethiol monolayer electrodes. CVs of nanoAu/MPA/Cyt c recorded at bare GC and Au/ET electrodes in deaerated aqueous PBS (pH 7.0) are shown in Fig. 2(A) and (B). The potential sweep rates are in a range of 0.02–5 V s^{-1}. The nano bioconjugate shows a reversible redox wave with a formal potential of 0.05 V (vs. Ag|AgCl) at both bare GC and Au/ET electrodes. The ratio of the cathodic and

Table 1
Formal potentials and peak-to-peak separation (ΔE_p) values of nanoAu-Cyt c conjugate at different electrodes recorded in deaerated aqueous PBS (25 mM, pH 7.0).

Electrode	Formal potential V (vs. Ag|AgCl)	ΔE_p (mV)
Au/ET	0.05	60
Au/BT	0.05	85
Au/MPA	0.06	115
Au/AET	0.06	130
Bare Au	0.06	170
Bare GC	0.05	70

the anodic peak currents of the redox wave is about 1 at each scan rate, and the peak-to-peak separation (ΔE_p) values are ~60–70 mV at slow scan rates. These observations clearly indicate that the nanobioconjuguate of Cyt c undergoes a reversible redox reaction. While Cyt c does not usually undergo direct electrodic reaction at bare electrodes in the absence of electron-transfer promoters [6–8,22,23], very recently a quasi-reversible redox response was observed for Cyt c by Mingot et al. at bare screen-printed graphite electrodes with no use of promoters or surface modifiers [24]. In our present study, we observed a facile reversible redox wave for Cyt c bound gold nanoconjugates at bare GC electrode and also at Au/ET monolayer electrode (Fig. 2(A) and (B)). Both the cathodic and the anodic peak currents are linearly proportional to the square root of scan rate, indicating that the electrochemical redox reaction of the nanoAu-Cyt c conjugates is a diffusion-limiting process. The observed formal potential (0.05 V) is only a little more positive than that of free Cyt c in solution (0.04 V) [25]. So, the nature of the heme protein, Cyt c, confined with the nanoparticles is likely equivalent to that of native Cyt c and would be possessing native tertiary structure and inherent chemical reactivity.

The formal potentials and peak-to-peak separation values of the redox reaction of nanoAu-Cyt c conjugate at different Au/alkanethiol and GC electrodes are given in Table 1. The formal potentials observed at most of the electrodes are nearly equivalent to that of solution-dissolved native Cyt c, and a variation of about +20 mV is observed depending on the nature of electrode. But, the peak-to-peak separation values obtained at 20 mV s^{-1} varied widely from 60 mV to 130 mV depending on the nature of the Au/alkanethiol working electrode and were as high as 170 mV at bare Au electrode. At Au/ET, Au/BT, and GC electrodes, the peak-to-peak separation values are nearly 60 mV. But at bare Au electrode and at Au/AET and Au/MPA monolayer electrodes having charged end groups, the peak-to-peak separation values are ~115–170 mV; further, the CVs deteriorate on repeated cycles and the peak-to-peak separation value increases further. These observations could be attributed to the fouling of electrode surface due to coagulation of the heme protein and its adsorption on the bare Au electrode and Au/thiol electrodes with charged end groups (Au/MPA and Au/AET electrodes). Thus for all further electrochemical and electrocatalytic experiments, the Au/ET electrode, exhibiting facile reversible redox reaction of nanoAu-Cyt c conjugate and covered with a monolayer of the short alkanethiol chain, is employed. Diffusion coefficient of the nanoparticles is determined from the peak currents of the redox waves of nanoAu/MPA/Cyt c at Au/ET electrode. From the slope of the plot of the peak current against the square root of scan rate, the apparent diffusion coefficient of the nanoparticles is determined to be 5.3×10^{-7} cm^2 s^{-1}. The diffusion coefficient of nanoAu-Cyt c is nearly 10 times lower than that reported for ferrocene bound to gold nanoparticles of ca. 1.5 nm [26]. According to Stokes–Einstein relation, the diffusion coefficient is inversely proportional to the square root of the diameter of the nanoparticles, and thus the determined diffusion coefficient of nanoAu-Cyt c conjugate of 3.0 nm diameter is quite reasonable with respect to the diffusion coefficient of the nanoAu-ferrocene conjugate.

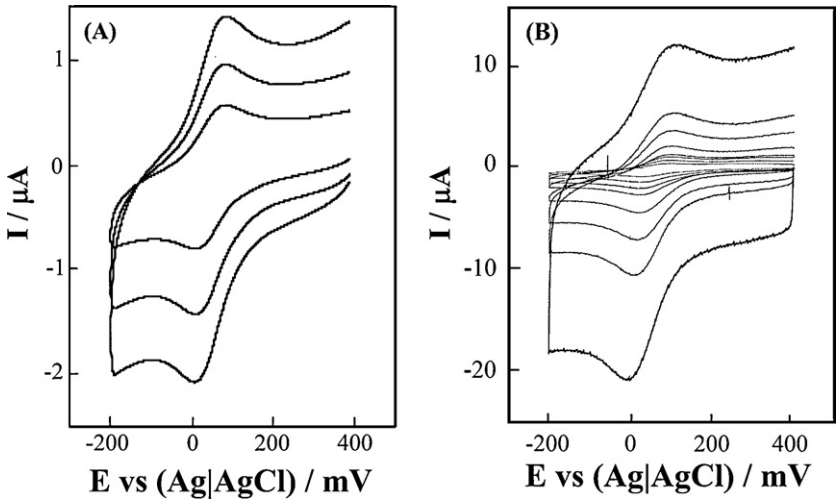

Fig. 2. CVs of nanoAu/MPA/Cyt c recorded at GC (A) and Au/ET (B) electrodes in deaerated aq. PBS (25 mM, pH 7.0) solution of nanoAu/MPA/Cyt c; concentration of nanoAu bound Cyt c is 0.08 mM. Potential scan rates were 0.02, 0.05, and 0.1 V s^{-1} (A) and 0.02, 0.05, 0.1, 0.2, 0.5, 1, 2, and 5 V s^{-1} (B).

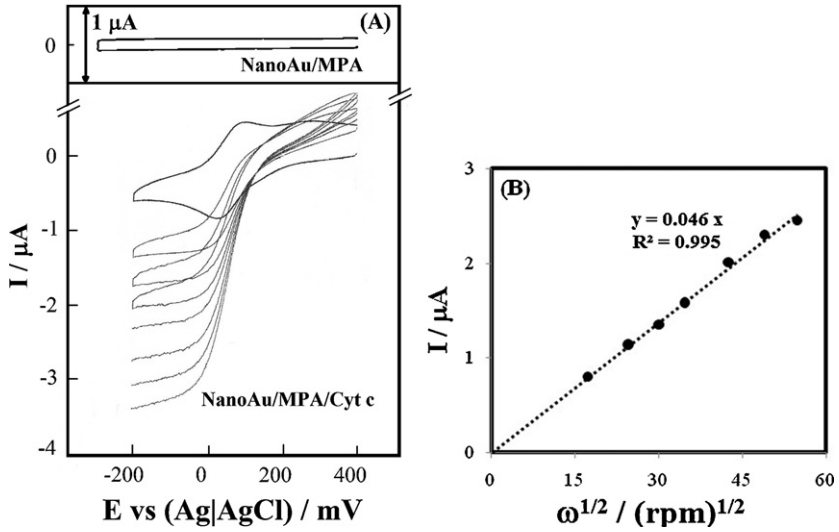

Fig. 3. A RDVs of nanoAu/MPA/Cyt c recorded at Au/ET electrode at a scan rate of 20 mV s^{-1}; disk-rotation rates are 0, 300–3000 rpm. Other conditions are same as in Fig. 2. Inset shows RDV of nanoAu/MPA recorded at Au/ET electrode (20 mV s^{-1}, 0 rpm). (B) Plot of the limiting current against the square root of rotation rate.

Rotating-disk voltammograms of the nanoAu/MPA/Cyt c conjugates were studied at different rotation rates of 300–3000 rpm in PBS (pH 7.0). The potential was scanned at 20 mV s^{-1}, and the obtained RDVs are shown in Fig. 3(A). At the redox potential of the conjugate (+0.05 V), a sharp increase in the cathodic current was observed and a plateau (I_{lim}) was attained at −0.1 V and further. In a control experiment, the CV of the nanoAu particle alone without Cyt c, i.e., nanoAu/MPA, was recorded at 0 rpm, and it is shown in the inset of Fig. 3(A). The CV of nanoAu/MPA showed no redox wave or no Faradaic current response, and only the double-layer charging current was observed (Fig. 3A inset). In the case of nanoAu/MPA/Cyt c conjugate, a predominant reversible redox wave is observed at +0.05 V; the weak anodic wave seen close to +300 mV is not usually observed and it could be due to the presence of a small fraction of Cyt c in a different chemical environment on the nanoparticle surface. For the nanoAu/MPA/Cyt c conjugate, the plot between the electrode potential and $\log[I/(I_{lim} - I)]$ at a given rotation rate shows a slope of about 60 mV, indicating that the number of electrons involved in the electrochemical redox reaction is 1 [27,28]. Previously nanoAu-ferrocene conjugates derivatized with a number of ferrocene moieties had also shown similar one-electron transfer redox process corresponding to a single ferrocene unit, despite the presence of several ferrocene units in the conjugate [26]. These RDV observations indicate that the electron-transfer to nanoAu-Cyt c conjugate involves with the transfer of only one-electron to nanoAu-Cyt c conjugate at the electrode-solution interface. Further, the limiting cathodic current response was found to increase with the rotation rate of the disk, and the limiting cathodic current intensity is linearly proportional to the square root of rotation rate (Fig. 3(B)). Thus the electrochemical redox reaction under hydrodynamic conditions is a facile mass-transport limited process.

3.3. Electrocatalytic detection of superoxide and SOD enzyme

Electrocatalytic response of the Cyt c bound nanoAu particles to the presence of superoxide radical and in turn for the quantification of superoxide dismutase enzyme are investigated by steady-state chronoamperometric analysis. Superoxide radical is generated by the enzymatic reaction of xanthine oxidase (XOD) with xanthine in oxygen-saturated solution. Electrocatalytic oxidation of

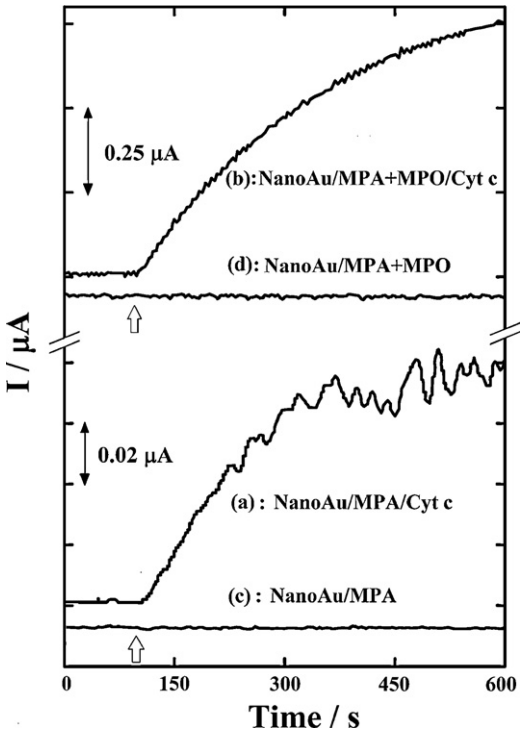

Fig. 4. Steady state current vs. time plots observed to the generation of superoxide radical by xanthine-XOD reaction at Au/ET electrode in oxygenated aq. PBS (25 mM, pH 7.0) solution containing nanoAu/MPA/Cyt c (a) or nanoAu/MPA + MPO/Cyt c (b); concentration of Cyt c in solution is 0.08 mM. Steady-state current vs. time plots observed in oxygenated PBS containing nanoAu/MPA (c) or nanoAu/MPA + MPO (d) without the bound Cyt c under identical conditions to the generation of superoxide.

superoxide radical at Au/ET electrode was investigated at the applied potential of +0.15 V in the presence of nanoAu/MPA/Cyt c and nanoAu/MPA + MPO/Cyt c. Fig. 4(a) shows the steady-state current–time curve observed at the Au/ET electrode in oxygen-saturated aq. PBS (pH 7.0) containing nanoAu/MPA/Cyt c and the solution is stirred at 200 rpm to perform the experiments under hydrodynamic conditions. Once a steady-state current response is attained at the electrode potential of +0.15 V, XOD enzyme is added at first to the electrolyte solution; after a brief time period of ~3 min, xanthine is added to a final concentration of 0.15 mM. On the addition of xanthine, the current increases gradually responding to the superoxide radical generated by xanthine-XOD reaction. It increased anodically and reached a plateau in about 6 min, and a current response of 0.07 μA (3.5 μA cm^{-2}) was observed. The anodic current response for the superoxide radical could be due to the electrocatalytic oxidation of superoxide radical by nanoAu-Cyt c conjugate. When nanoAu/MPA + MPO/Cyt c particles were used instead of nanoAu/MPA/Cyt c, the anodic current response was nearly 12 times higher than that observed with nanoAu/MPA/Cyt c (Fig. 4(b)). The current increased anodically on the addition of xanthine and reached a plateau in about 6 min. The observed current intensity was as high as 0.90 μA (45 μA cm^{-2}). Control experiments for the response of the nanoAu particles without the bound Cyt c to superoxide radical were carried out. Steady-state current vs. time plots observed with nanoAu/MPA and nanoAu/MPA + MPO particles to the generation of superoxide radical by the addition of xanthine are shown in Fig. 4(c) and (d). In the control experiments, the current vs. time plots showed negligible response to the generation of superoxide radical (Fig. 4(c) and (d)). These observations clearly confirm that the electrocatalytic oxidation of superoxide radical occurs due to the presence of covalently bound Cyt c in the nanoAu bioconjugates.

The cause for the large increase in the current response for the electrocatalytic oxidation of superoxide by employing the binary monolayer based nanoAu bioconjugate, nanoAu/MPA + MPO/Cyt c, is not clear. However, it could be attributed to the difference in the heterogeneous electron-transfer rates reported previously for Cyt c immobilized on Au electrodes modified with different monolayer and binary mixed-monolayer of alkanethiols. The heterogeneous electron-transfer rate of Au/MPA/Cyt c and Au/MPA + MPO/Cyt c were determined by CV experiments and were 12 s^{-1} and 2800 s^{-1}, respectively [29]. The heterogeneous electron-transfer rates reported previously for Cyt c immobilized on simple Au/alkanethiol monolayer electrodes (alkanethiol = MPA, mercaptohexadecanoic acid, etc.) were found to be dependent on the alkanethiol chain-length and were about 0.4–880 s^{-1} [30–36]. The heterogeneous electron-transfer rate decreases with the increase in alkanethiol chain-length [35,37]. For the long chain alkanethiol electrode, Au/MUDA/Cyt c (MUDA = 11-mercapto-1-undecanoic acid), the electron-transfer rates were reported to be 1.7–23 s^{-1} [30,33], and for the short chain alkanethiol electrode, Au/MPA/Cyt c, it was as high as 880 s^{-1} [35]. Further, the heterogeneous electron-transfer rate enhanced with the use of binary mixed-monolayer electrodes and was as high as 73 s^{-1} for Au/MUDA + MU/Cyt c (MU = 11-mercapto-1-undecanol) [32,33]. Thus, the reported electron transfer rate of 2800 s^{-1} at the binary monolayer-based electrode, Au/MPA + MPO/Cyt c, is highly reasonable, considering the short chain-length of the MPA layer [29]. Further, the electron-transfer rates of simple Au/MUDA/Cyt c were found to be increased in the presence of nanoAu particles [16]. Because of such efficient heterogeneous electron-transfer rates with the use of mixed-monolayer and nanoAu particles, the electrocatalytic current for the superoxide radical could have increased with the use of binary mixed-monolayer based nanobioconjugate, nanoAu/MPA + MPO/Cyt c (Fig. 4). The observed results clearly emphasize that *not simply the nanoAu particles but also the surface morphology and interfacial characteristics of nanoAu particles played vital role* in the electron-transfer characteristics.

Superoxide dismutase is a selective and potential scavenger of superoxide radical and its presence in the solution would catalyze dismutation of superoxide radical. The electrocatalytic current response for the superoxide radical would thus respond by a decrease to the presence of SOD enzyme and in turn the concentration of the enzyme could be detected. The electrocatalytic current observed with nanoAu/MPA/Cyt c (70 nA) is quite little and is only about 10 times higher than the baseline noise of the electrochemical analyzer. Thus, nanoAu/MPA/Cyt c could not be investigated for the detection of SOD enzyme. The anodic current response to the generation of superoxide radical with nanoAu/MPA + MPO/Cyt c bioconjugate was investigated in the presence and absence of SOD at different concentrations. The current–time plots observed in the presence and absence of SOD enzyme (0–5 U mL^{-1}) are shown in Fig. 5(A), and the electrocatalytic current for superoxide radical was found to decrease with the presence of 1 U mL^{-1} SOD enzyme ((a) and (b)). The electrocatalytic current decreases further with increasing concentrations of SOD enzyme (Fig. 5(A), b–d). The electrocatalytic experiments were repeated for at least three times with independent electrodes, and the observed change in the electrocatalytic current is plotted against the concentration of SOD enzyme (Fig. 5(B)). The current response was reproducible with a relative standard deviation (RSD) of ±0.02 μA. The low-detection-limit (LDL) of the sensor, which is three RSDs higher than the basic current observed in the absence of SOD, is calculated from the graph Fig. 5(B) by using the following equation, LDL = [3 × RSD/slope] + C_{lo}, to be 0.25 U mL^{-1} (i.e., ~50 ng mL^{-1}). The low-detection-limit determined is highly comparable to those reported previously. The low-detection-limit of a hemin-modified pyrolytic graphite electrode was earlier reported to be 0.02 U mL^{-1}

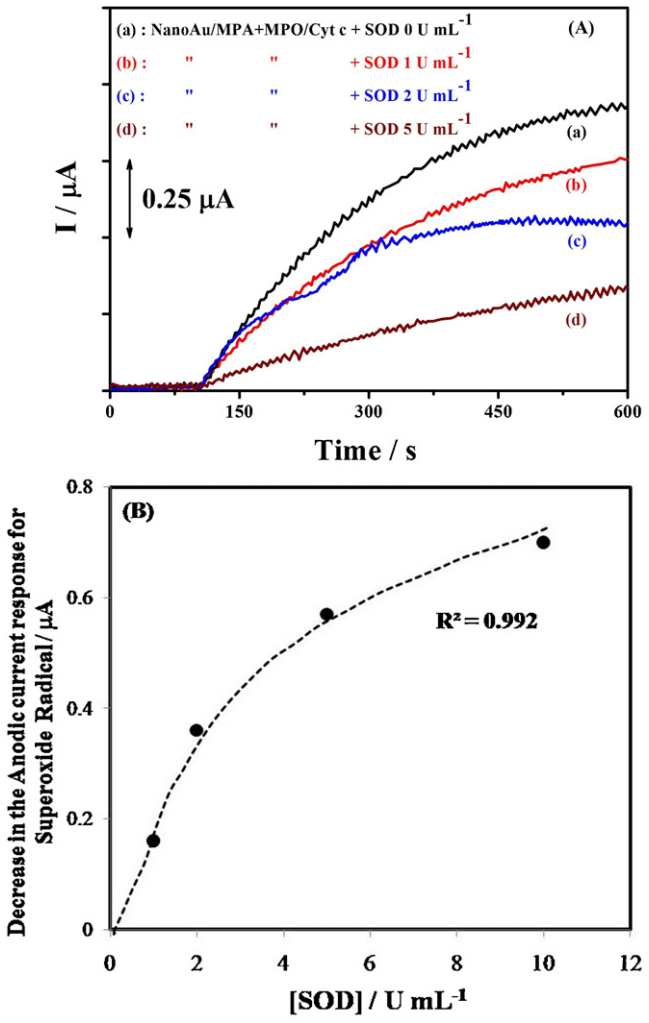

Fig. 5. A Steady state current vs. time plots obtained to the addition of SOD at different concentrations in oxygenated aq. PBS containing nanoAu/MPA + MPO/Cyt c. Other conditions are same as in Fig. 4. (B) Plot between the decrease in anodic current response for superoxide against the concentration of SOD.

SOD [38]. At Au/MPA + MPO/Cyt c electrode, the detection limit was as low as 0.01 U mL^{-1} SOD [29]. The detection limit obtained in this investigation is better compared to standard photometric investigations, where the detection limit is 0.05 U mL^{-1} [39].

4. Conclusions

An amperometric biosensor based on nanoAu-Cyt c bioconjugate for the detection of SOD was developed in this study, and it was highly sensitive to the presence of as low as 0.25 U mL^{-1} (~50 ng mL^{-1}) with a response time of ~6 min. Interfacial alkanethiol monolayer of the nanoAu-Cyt c bioconjugate was found to play an important role in the electrocatalytic current response of the sensor system. The increase in the anodic current response for superoxide radical as high as 12 times with the presence of a binary mixed-monolayer of alkanethiols at the interface of the nanoAu-Cyt c conjugate *further emphasizes the importance of fine-tuning the interfacial structure and morphology even at nanomaterial levels*. To the best of our knowledge, this is the first time such a large difference in the electrocatalytic characteristics were reported by changing the surface characteristics of nanoAu particles with different alkanethiolate monolayers. Such nanoAu conjugates of similar electroactive proteins could be prepared to achieve facile heterogeneous electron-transfer reaction directly at bare electrodes and to fabricate efficient three-dimensional electrochemical sensor systems. Electrocatalytic investigations with the use of three-dimensional matrices of nanoAu-Cyt c bioconjugates are under investigation for reducing the response time.

Acknowledgments

The authors gratefully acknowledge the National Institute of Advanced Industrial Science and Technology (NIAIST), Tsukuba, Japan for nanoAu samples and TEM imaging. K. Koteshwara Reddy acknowledges gratefully the National Institute of Technology, Warangal and the Ministry of Human Resource Development, Government of India for his Junior Research Fellowship and financial support.

References

[1] M.K. Beissenhirtz, F.W. Scheller, M.S. Viezzoli, F. Lisdat, Analytical Chemistry 78 (2006) 928.
[2] J.R. Henderson, H. Swalwell, S. Boulton, P. Manning, C.J. McNeil, M.A.B. Machin, Free Radical Research 43 (2009) 796.
[3] J. Xue, Y. Xian, X. Ying, J. Chen, L. Wang, L. Jin, Analytica Chimica Acta 405 (2000) 77.
[4] F. Darain, J.S. Park, H. Akutsu, Y.B. Shim, Biosensors and Bioelectronics 23 (2007) 161.
[5] X. Zhang, H. Ju, J. Wang, Electrochemical Sensors, Biosensors and their Biomedical Applications, Academic Press, 2008.
[6] X.J. Chen, A.C. West, D.M. Cropek, S. Banta, Analytical Chemistry 80 (2008) 9622.
[7] M.C. Puig, X.M. Berbel, C.C. Blanchard, J.L. Marty, Talanta 79 (2009) 289.
[8] X. Ji, J. Ren, J. Jin, T. Nakamura, Biosensors and Bioelectronics 23 (2007) 241.
[9] Z. Guo, J. Chen, H. Liu, W. Zhang, Analytical Letters 38 (2005) 2033.
[10] H. Liu, Y. Tian, P. Xia, Langmuir 24 (2008) 6359.
[11] A. Salimi, A. Noorbakhsh, H.A.R. Pour, H. Ghourchian, Electroanalysis 23 (2011) 683.
[12] S. Rajesh, A.K. Kanugula, K. Bhargava, G. Ilavazhagan, S. Kotamraju, C. Karunakaran, Biosensors and Bioelectronics 26 (2010) 689.
[13] J. Di, S. Peng, C. Shen, Y. Gao, Y. Tu, Biosensors and Bioelectronics 23 (2007) 88.
[14] Y. Wang, Y. Wu, J. Wang, J. Di, Bioprocess and Biosystems Engineering 32 (2009) 531.
[15] M.K. Beissenhirtz, F.W. Scheller, F. Lisdat, Analytical Chemistry 76 (2004) 4665.
[16] K. Caban, A. Offenhausser, D. Mayer, Physical Status Solidi A 206 (2009) 489.
[17] P.S. Jensen, Q. Chi, F.B. Grumsen, J.M. Abad, A. Horsewell, D.J. Schiffrin, J. Ulstrup, Journal of Physical Chemistry C 111 (2007) 6124.
[18] A. Zhu, Y. Tian, H. Liu, Y. Luo, Biomaterials 30 (2009) 3183.
[19] D.H. Nagaraju, R.K. Pandey, V. Lakshminarayanan, Journal of Electroanalytical Chemistry 627 (2009) 63.
[20] Y. Wang, X. Ma, Y. Wen, Y. Xing, Z. Zhang, H. Yang, Biosensors and Bioelectronics 25 (2010) 2442.
[21] M. Brust, M. Walker, D. Bethell, D. Schiffrin, R. Whyman, Journal of the Chemical Society, Chemical Communications 7 (1994) 801.
[22] B.J. Plowman, M. Mahajan, A.P. O'Mullane, S.K. Bhargava, Electrochimica Acta 55 (2010) 8953.
[23] Y. Zhang, J. Zheng, Electrochimica Acta 54 (2008) 749.
[24] M.G. Mingot, J. Iniesta, V. Montiel, R.O. Kadara, C.E. Banks, Analyst 136 (2011) 2146.
[25] F.M. Hawkridge, T. Kuwana, Analytical Chemistry 45 (1973) 1021.
[26] S.J. Green, J.J. Pietron, J.J. Stokes, M.J. Hostetler, H. Vu, W.P. Wuelfing, R.W. Murray, Langmuir 14 (1998) 5612.
[27] A.J. Bard, L.R. Faulkner, Electrochemical Methods, Wiley, Singapore, 2004.
[28] R.G. Compton, C.E. Banks, Understanding Voltammetry, World Scientific, Singapore, 2009.
[29] K.V. Gobi, F. Mizutani, Journal of Electroanalytical Chemistry 484 (2000) 172.
[30] Y. Li, J. Li, X.H. Xia, S.Q. Liu, Talanta 82 (2010) 1164.
[31] Y.C. Liu, S.Q. Cui, J. Zhao, Z.S. Yang, Bioelectrochemistry 70 (2007) 416.
[32] M.C. Puig, X.M. Berbel, R. Rouillon, C.C. Blanchard, J.L. Marty, Bioelectrochemistry 76 (2009) 76.
[33] B. Ge, F. Lisdat, Analytica Chimica Acta 454 (2002) 53.
[34] S. Song, R.A. Clark, E.F. Bowden, Journal of Physical Chemistry 97 (1993) 6564.
[35] Z.Q. Feng, S. Imabayashi, T. Kakiuchi, K. Niki, Journal of Electroanalytical Chemistry 394 (1995) 149.
[36] Z.Q. Feng, S. Imabayashi, T. Kakiuchi, K. Niki, Journal of Electroanalytical Chemistry 408 (1996) 15.
[37] R.A. Marcus, N. Sutin, Biochimica et Biophysica Acta 811 (1985) 265.
[38] J. Chen, U. Wollenberger, F. Lisdat, B. Ge, F.W. Scheller, Sensors and Actuators B 70 (2000) 115.
[39] J.M. McCord, I. Fridovich, Journal of Biological Chemistry 244 (1969) 6049.